

Flow Control in a Driven Cavity Incorporating Excitation Phase Differential

Kristin Fitzpatrick,* Yunfei Feng,[†] Rick Lind,[‡] Andrew J. Kurdila,[§] and David W. Mikolaitis[¶]
University of Florida, Gainesville, Florida 32611

Control of fluid flow is particularly difficult because of inherent nonlinearity in the Navier–Stokes equations and high dimensionality of typical approximations of these equations. A control design is demonstrated for flow restricted to creeping flow within a driven cavity. Such a restriction allows linear reduced-order models to be generated as state-space systems. In particular, these models are generated as subspaces of the flow where each model represents modes associated with phase differential between exogenous disturbances. A linear parameter-varying controller is designed to account for the range of dynamics introduced by the phase differential among subspaces. The controller is introduced to the reduced-order models, which contain individual phase-differential subspaces, and the full-order model, which contains all phase-differential subspaces, for disturbance attenuation. These closed-loop simulations show that the gain-scheduled controller, designed for individual subspaces, is able to reduce the flow velocity along the centerline of the cavity significantly for the full-order flow.

Nomenclature

A	= state matrix
B	= input/excitation matrix
C	= output/observability matrix
D	= feedthrough matrix
f	= characteristic frequency
g_i	= boundary functions
$h_0(t)$	= velocity along top boundary
K	= controller
L	= characteristic dimension
P	= plant
Re	= Reynolds number
St	= Strouhal number
V_m	= mean velocity at top boundary
V_s	= characteristic velocity
V_0	= static Stokes flow at top boundary
W_h	= top disturbance input filter
W_k	= control weighting
W_n	= noise weighting
W_p	= performance weighting
W_u	= command input filter
W_y	= sensor measurements output filter
α	= original reduced-state variables
$\beta(t)$	= velocity along bottom boundary
$\beta\Psi$	= control basis
Γ	= boundary condition
δ	= phase differential parameter

Φ	= flow shape basis
Ω	= flow domain

I. Introduction

RESEARCH into flow control techniques has been continually evolving as related technologies mature. These technologies include hardware development, such as sensors and actuators,¹ and software development, such as models and simulations,² associated with fluid dynamics. In each case, the technologies are being developed with careful consideration of the requirements for control design and implementation.³

A particular challenge for flow control has been the development of open-loop models for which controllers can be designed. The primary difficulty lies with the inherent nonlinearity of the Navier–Stokes equations that govern the fluid flow. Approximations of these equations can have large dimensionality. Within the last decade, studies of flow control have addressed specific flow regimes. These regimes include the control of a driven cavity by the use of linear quadratic regulator (LQR) control,⁴ the use of piezoceramic actuators to control a channel flow,⁵ and the use of synthetic jets for flow control.⁶ These applications demonstrate control for relatively simple systems, but no method of control design exists that can directly utilize the full-order dynamics of a realistic flow.

A considerable amount of attention has been devoted in recent years to generate reduced-order flow models. Two specific techniques that employ a reduced basis are proper orthogonal decomposition (POD)⁷ and fluid mode methods.³ POD is a model reduction technique in which the most energetic modes are systematically extracted from numerical simulations. This method of reduction was used to create the models used in this paper. The fluid mode method uses basis functions that are closely related to the physics of the problem being solved.

A recent study has shown that models can indeed be generated that are amenable to control a specific type of flow.⁸ The system in that study is restricted to creeping flow in a driven cavity. Specifically, the left and right sides of the cavity have zero flow velocity, whereas the top and bottom boundaries are driven by exogenous flow with fixed velocity and frequency. Models are generated by the consideration of the linearized dynamics associated with modes obtained via POD.⁹ These modes were used to derive controllers for disturbance rejection. The derived controllers were able to keep the flow nearly stationary at various points throughout the cavity for varying flow regime, despite the exogenous input.^{4,10}

This paper extends a previous work⁸ to consider different flow conditions for the driven cavity. Specifically, open-loop models are generated by consideration of the phase differential between the

Presented as Paper 2003-5350 at the AIAA Guidance, Navigation, and Control Conference, Austin, TX, 11 August 2003; received 18 August 2003; revision received 20 January 2004; accepted for publication 21 January 2004. Copyright © 2004 by the authors. Published by the American Institute of Aeronautics and Astronautics, Inc., with permission. Copies of this paper may be made for personal or internal use, on condition that the copier pay the \$10.00 per-copy fee to the Copyright Clearance Center, Inc., 222 Rosewood Drive, Danvers, MA 01923; include the code 0731-5090/05 \$10.00 in correspondence with the CCC.

*Graduate Student, Department of Mechanical and Aerospace Engineering; frogy@ufl.edu. Student Member AIAA.

[†]Graduate Student, Department of Mechanical and Aerospace Engineering; fengyf@mae.ufl.edu.

[‡]Assistant Professor, Department of Mechanical and Aerospace Engineering; rick@mae.ufl.edu. Senior Member AIAA.

[§]Professor, Department of Mechanical and Aerospace Engineering; ajk@mae.ufl.edu. Associate Fellow AIAA.

[¶]Associate Professor, Department of Mechanical and Aerospace Engineering; dwm@mae.ufl.edu. Senior Member AIAA.

disturbances at the top and bottom of the cavity. The previous study introduced an open-loop model that represented the flow conditions for a phase differential of 180 deg between the upper and lower disturbances. In reality, the upper and lower boundaries will vary across a wide range of phase differentials. This paper will introduce reduced-order models of the cavity flow associated with upper and lower boundaries that are 210, 195, 180, 165, and 150 deg different in phase to account for a realistic range of flow conditions.

A linear parameter-varying (LPV) controller is designed for the models corresponding to the range of various phase differentials. The group of models can be considered to lay within a parameter space, with the parameter being the phase differential between the excitation and disturbance. In this way, a controller is designed that varies with the phase differential noted in the flow.

The objective of this paper is to demonstrate a methodology for flow control based on subspaces. Essentially, each reduced-order model is generated for a particular phase differential and, thus, represents a subspace of the full-order flow. The LPV controller is scheduled across phase differential, thus, it is actually scheduled across subspaces. A closed-loop simulation of the full-order model, which contains many phase differentials, is used to demonstrate the applicability of the approach. The controller is able to satisfy the performance objectives on multiple reduced-order models, representing individual subspaces, and also on the single full-order model, representing the combination of all subspaces, for the cavity flow.

The control design is demonstrated on Stokes, or creeping, flow within a cavity. The use of Stokes flow limits the flow to being incompressible with Reynolds number less than one. One side effect of lowering a flow's Reynolds number is that the acceleration term within the Navier–Stokes governing equation becomes small compared to the viscous force term. This change allows the equation to be simplified into the linear Stokes equation.^{11,12} Thus, creeping flow within a cavity provides an excellent system for demonstrating the methodology of LPV control.

II. Driven Cavity Geometry

This paper will investigate flow control for a cavity, shown in Fig. 1, where $h_0(t)$ is the velocity along the top of the cavity, $\beta(t)$ is the velocity along the bottom of the cavity, and $\Gamma = \Gamma_L \cup \Gamma_R \cup \Gamma_T \cup \Gamma_B$ is the boundary of the domain. This cavity is enclosed by rigid walls with no-slip boundary conditions on the right and left sides. The top and bottom, however, have nonzero boundary conditions, in general.

The flow at the top and bottom boundaries have uniform spatial distribution. This restriction implies that the flow at any point along the upper boundary is identical to the flow at any other point along the upper boundary. Similarly, the flow at any point along the bottom boundary is identical to the flow at any other point along the bottom boundary. Such a perfect distribution is not possible because of the singularity at the points on the corners where the flow is moving on the horizontal boundary, but is stationary on the vertical boundary. Such a situation is obviously an approximation, but this example does serve as an initial problem to demonstrate the methodology.

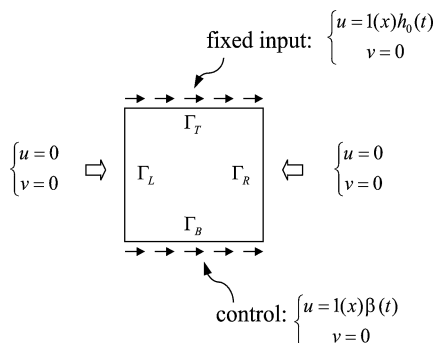


Fig. 1 Stokes driven cavity flow problem.

The approximation within the two-dimensional cavity is based on a grid with an index of 21 by 21 points. It is assumed that the measurements of the flow velocity are taken at 19 points along the horizontal centerline of the cavity, with the outer points lying one grid point away from the closest boundary wall. These measurements only provide the horizontal velocity of the flow. Also, the sensors generating these measurements are assumed to exist within the cavity without altering the flow. Again, such a situation is obviously an approximation, but the example serves to demonstrate the methodology.

III. Nonlinear Dynamics

This section derives the reduced-order models of the creeping flow within a driven cavity. The derivations presented here are actually an outline taken from a rigorous presentation in the references.⁸

A. Governing Equations of Motion

Consider first the unsteady Navier–Stokes equations

$$\rho \frac{\partial \mathbf{V}}{\partial t} + \rho \mathbf{V} \cdot \nabla \mathbf{V} = -\nabla p + \mu \Delta \mathbf{V}$$

subject to boundary conditions described in the past section. The parameter \mathbf{V} is the velocity field, p is the pressure, ρ is the density, and μ is the viscosity of the fluid. The constants that will be used to nondimensionalize the problem include a characteristic dimension L , characteristic velocity V_s , and characteristic frequency f . We define the following nondimensional variables:

$$\begin{aligned} x^* &= x/L, & y^* &= y/L, & \mathbf{V}^* &= \mathbf{V}/V_s \\ p^* &= p/\rho L V_s, & t^* &= t f \end{aligned}$$

We can write the resulting nondimensional Navier–Stokes equation as

$$Re \cdot Sr \frac{\partial \mathbf{V}^*}{\partial t^*} + Re(\mathbf{V}^* \cdot \nabla^* \mathbf{V}^*) = -Re \cdot Sr \nabla^* p^* + \Delta^* \mathbf{V}^*$$

where Sr is Strouhal number defined as

$$Sr = Lf/V_s$$

Define

$$\lambda = Re \cdot Sr = \rho L^2 f / \mu$$

This paper will consider flow such that $\lambda \sim \mathcal{O}(1)$ and the Reynolds number is $Re = 0.1$. In this case, the terms on the right-hand side will balance the first term on the left-hand side and the second term will be neglected.

Define the constant

$$\theta = 1/\lambda = 1/(Re \cdot Sr)$$

Finally, we get the governing equations for the approximation of Stokes flow

$$\frac{\partial \mathbf{V}^*}{\partial t^*} - \theta \Delta \mathbf{V}^* + \nabla \hat{p} = 0 \quad (1)$$

For convenience, we will write the preceding equation as

$$\frac{\partial \mathbf{V}}{\partial t} - \theta \Delta \mathbf{V} + \nabla p = 0 \quad (2)$$

while keeping in mind that these are nondimensional variables.

B. Reduced-Order Linear Dynamics

For the geometry depicted in Fig. 1, define the flow domain as Ω . The boundary of the fluid flow domain is given by

$$\partial\Omega = \Gamma_T \cup \Gamma_B \cup \Gamma_L \cup \Gamma_R$$

It is assumed that the input velocity imparted by the moving wall can be represented in term of N_c functions \mathbf{g}_i , $i = 1, \dots, n_c$. Each of the functions \mathbf{g}_i are defined on the entire domain Ω , but are assumed to exhibit specific properties on the boundary. We require that

$$\mathbf{g}_i|_{\partial\Omega}(x) = \begin{cases} 1 & \text{for } x \in \Gamma_B \\ 0 & \text{for } x \in \partial\Omega \setminus \Gamma_B \end{cases}$$

We additionally require that

$$\int_{\partial\Omega} \mathbf{g}_i \cdot \hat{n} \, dS = 0$$

for $i = 1, \dots, N_c$. This last condition is required to guarantee compatibility of the flowfield with the continuity equation.

The dynamics for incompressible, two-dimensional creeping flows can be represented in the strong form of Stokes equation by rewriting Eq. (2).

$$\frac{\partial \mathbf{V}}{\partial t} - \theta \Delta \mathbf{V} + \nabla p = \mathbf{f}$$

Likewise, the strong form of the continuity equation for incompressible flow is

$$\nabla \cdot \mathbf{V} = 0$$

In these equations, \mathbf{V} is the flow velocity, p is the pressure, and \mathbf{f} is the body force. We assume that spatially varying functions Φ_i , for $i = 1, \dots, N_s$ have been determined from the POD procedure, which will be discussed in detail later. The functions ϕ_i constitute the reduced basis used to represent the N_s states in the control model, which include phase differential information. There is a different set of ϕ_i functions associated with each parameter within the phase differential subspace $\delta = [150, 210]$, which is used to create reduced-order models at specific phase differentials. Similarly, we assume that spatially varying functions \mathbf{g}_i , for $i = 1, \dots, N_c$, have likewise been derived from a simulation or experiment. The functions \mathbf{g}_i comprise the influence functions that determine the controls acting on the fluid flow. It is assumed that these functions satisfy the following conditions, which are conventional in many reduced basis formulations:

$$\begin{aligned} \nabla \cdot \phi_i &= 0, & i &= 1, \dots, N_s \\ \nabla \cdot \mathbf{g}_i &= 0, & i &= 1, \dots, N_c \\ \phi_i|_{\partial\Omega} &= 0, & i &= 1, \dots, N_s \\ \mathbf{g}_i &= 0, & \text{for } x &\notin \Gamma_B \end{aligned}$$

In terms of these reduced basis functions, the velocity appearing in the Stokes equations is assumed to take the form

$$\mathbf{V}(x, y, t) = \mathbf{V}_M(t) + \sum_{i=1}^{N_c} \mathbf{g}_i(x, y) \beta_i(t) + \sum_{i=1}^{N_s} \phi_i(x, y) \alpha_i(t)$$

To derive a reduced-order model appropriate for control synthesis, it is necessary to convert the strong form of the governing equations to weak form. We define the inner product, bilinear form $a(\cdot, \cdot)$, respectively, as

$$\begin{aligned} (\mathbf{u}, \mathbf{v})_{[L^2(\Omega)]^2} &\triangleq \sum_{i=1}^2 \int_{\Omega} u_i v_i \, dx \\ a(\mathbf{u}, \mathbf{v}) &\triangleq \theta \sum_{i=1}^2 \sum_{j=1}^2 \int_{\Omega} \frac{\partial u_i}{\partial x_k} \frac{\partial v_j}{\partial x_k} \, dx \end{aligned}$$

By substituting the velocity into the strong form of the governing equations, taking the inner product of the resulting expression with an arbitrary basis function ϕ_i , and integrating over the domain Ω , we obtain

$$\begin{aligned} &\left[\sum_{i=1}^{N_c} \mathbf{g}_i(x, y) \dot{\beta}_i(t) + \sum_{i=1}^{N_s} \phi_i(x, y) \dot{\alpha}_i(t), \phi_j \right]_{[L^2(\Omega)]^2} \\ &+ a \left[\mathbf{V}_M + \sum_{i=1}^{N_c} \mathbf{g}_i(x, y) \beta_i(t) + \sum_{i=1}^{N_s} \phi_i(x, y) \alpha_i(t), \phi_j \right] \\ &= (\mathbf{f}, \phi_j)_{[L^2(\Omega)]^2} \end{aligned}$$

We can gather terms and put the equations in a canonical form appropriate for control synthesis:

$$\begin{aligned} &\sum_{i=1}^{N_c} (\mathbf{g}_i, \phi_j)_{[L^2(\Omega)]^2} \dot{\beta}_i(t) + \sum_{i=1}^{N_s} (\phi_i, \phi_j)_{[L^2(\Omega)]^2} \dot{\alpha}_i(t) + a(\mathbf{V}_M, \phi_j) \\ &+ \sum_{i=1}^{N_c} a(\mathbf{g}_i, \phi_j) \beta_i(t) + \sum_{i=1}^{N_s} a(\phi_i, \phi_j) \alpha_i(t) = (\mathbf{f}, \phi_j)_{[L^2(\Omega)]^2} \end{aligned}$$

We define a new set of states that include both the original reduced-state variables and the amplitude of the controls

$$X(t) = \begin{Bmatrix} \alpha(t) \\ \beta(t) \end{Bmatrix}$$

The new set of controls is defined to be the time derivative of the original controls

$$u(t) = \{\dot{\beta}(t)\}$$

With these definitions of the state $X(t)$ and controls $u(t)$, it is possible to write the weak form of the governing equations as

$$[\tilde{M}] \dot{X}(t) = [\tilde{A}] X(t) + [\tilde{B}] u(t) + [\tilde{C}(t)]$$

Note that the matrix $[\tilde{M}]$ will be diagonal if the reduced basis vectors are derived from a POD. We can obtain the final form of the reduced-state equations by premultiplying by the inverse of the matrix $[\tilde{M}]$:

$$\dot{X}(t) = [\tilde{M}]^{-1} [\tilde{A}] X(t) + [\tilde{M}]^{-1} \tilde{Q} [X(t)] + [\tilde{M}]^{-1} [\tilde{B}] u(t)$$

which can be rewritten in the final form as

$$\dot{X}(t) = [A(\theta)] X(t) + [B] u(t) + [E(\theta, t)] \quad (3)$$

where $[A(\theta)]$ is a linear function of θ , $[B]$ is a constant matrix, and $[E(\theta, t)]$ is a function of $h_0(t)$.

C. Creeping Flow in a Driven Cavity

Because the dynamic model is linear, we can construct $\mathbf{V}_M(t)$ as

$$\mathbf{V}_M(t) = \mathbf{V}_0 \cdot h_0(t)$$

where \mathbf{V}_0 is the velocity field of creeping flow when constant horizontal velocity is imposed on the top of the cavity. We require that

$$\mathbf{V}_0|_{\partial\Omega}(x) = \begin{cases} 1 & \text{for } x \in \Gamma_T \\ 0 & \text{for } x \in \partial\Omega \setminus \Gamma_T \end{cases}$$

Also, we choose $N_c = 1$ and \mathbf{g} as the velocity field that corresponds to a constant horizontal velocity imposed on the bottom wall of the cavity. We require that

$$\mathbf{V}_0|_{\partial\Omega}(x) = \begin{cases} 1 & \text{for } x \in \Gamma_B \\ 0 & \text{for } x \in \partial\Omega \setminus \Gamma_B \end{cases}$$

The velocity can subsequently be decomposed as

$$\mathbf{V}(x, y, t) = \mathbf{V}_0 h_0(t) + \mathbf{g}(x, y)\beta(t) + \sum_{i=1}^{N_S} \phi_i(x, y)\alpha_i(t)$$

Thus, the reduced-order model in Eq. (3) can be rewritten explicitly as

$$\begin{aligned} \begin{Bmatrix} \dot{\alpha} \\ \dot{\beta} \end{Bmatrix} &= \begin{bmatrix} [A_1(\theta)] & [A_2(\theta)] \\ 0 & 0 \end{bmatrix} \begin{Bmatrix} \alpha \\ \beta \end{Bmatrix} \\ &+ \begin{bmatrix} [E_1(\theta)] & [E_2] \\ 0 & 0 \end{bmatrix} \begin{Bmatrix} h_0 \\ \dot{h}_0 \end{Bmatrix} + \begin{bmatrix} [B_1] \\ 1 \end{bmatrix} \dot{\beta} \end{aligned} \quad (4)$$

Consider just the partition associated with the time-domain equation for α ,

$$\dot{\alpha} = A_1(\theta)\alpha(t) + A_2(\theta)\beta(t) + B_1\dot{\beta}(t) + E_1(\theta)h_0(t) + E_2\dot{h}_0(t)$$

Formulate the equivalent frequency-domain expression

$$s\alpha(s) = A_1(\theta)\alpha(s) + A_2(\theta)\beta(s) + sB_1\beta(s) + E_1(\theta)h(s) + sE_2h(s)$$

We can now solve for a transfer function representation of the inputs to outputs:

$$\begin{aligned} \alpha(s) &= \frac{sE_2 + E_1(\theta)}{s - A_1(\theta)}h_0(s) + \frac{sB_1 + A_2(\theta)}{s - A_1(\theta)}\beta(s) \\ &= \begin{bmatrix} A_1(\theta) & E_1(\theta) + A_1(\theta)E_2 \\ I & E_2 \end{bmatrix} h(s) + \begin{bmatrix} A_1 & A_2 + A_1B_1 \\ I & B_1 \end{bmatrix} \beta(s) \\ &= \begin{bmatrix} A_1(\theta) & E_1(\theta) & A_2(\theta) \\ I & E_2 & B_1 \end{bmatrix} \begin{Bmatrix} h(s) \\ \beta(s) \end{Bmatrix} = P(s) \begin{Bmatrix} h(s) \\ \beta(s) \end{Bmatrix} \end{aligned} \quad (5)$$

The reduced-order model described by P is a fairly accurate representation of the open-loop dynamics for Stokes flow in the driven cavity with $\theta \sim \mathcal{O}(1)$. All of the models will be based on a $\theta = 1$ in this paper. There is a decrease in accuracy as θ changes from unity because of unmodeled nonlinearities. The LPV controller is designed and tested for models over the range of phase differentials $\delta = [150, 210]$.

IV. Excitation Phase Differential

Open-loop models of the flow dynamics are generated by analysis of the simulated responses of the driven cavity. This simulation uses the Stokes flow as the fluid dynamics. Separate models are generated for each set of flow conditions that corresponded to different relationships between the upper and lower boundaries.

Each of these models have physical limitations associated with them. The Reynolds number for each model is $Re = 0.1$. The combination of the low Reynolds number and the approximation of the Navier–Stokes equation creates a flow that is dominated by viscous effects.

The fluid at the upper and lower boundaries was constrained to move at a sinusoidal frequency with constant amplitude. The frequency of this sinusoidal is essentially considered a nondimensional unity because the timescales in the dynamics are all normalized. This excitation acts as a disturbance that affects the entire flow within the cavity.

The variations between the flow conditions used for model development were phase relationships between the upper and lower boundaries. Specifically, the sinusoidal flows differed in phase by 210, 195, 180, 165, and 150 deg between the upper and lower boundaries. These phase differences induced different modal structures within the flow so that the various models were generated to represent a basis for this range of flow conditions.

The reduced-order models associated with each phase differential, which contain three states, can actually be considered as subspaces of the full-order flow, which contains 623 states. The exogenous disturbances will, in general, not have a constant phase

differential, and so the flowfield will contain modes associated with many phase differentials throughout any time evolution. As such, each reduced-order model represents a subspace of the modes observed in that full-order flowfield. Thus, the synthesis of controllers for these models with phase differentials is essentially the design compensators that are optimal with respect to each subspace.

V. Control Design

A. Control Objectives

The objective of flow control in this paper is to reject the effects of the exogenous disturbance at the top of the driven cavity. Physically, the control seeks to minimize the horizontal component of the fluid velocity at a set of sensor locations. These sensors are located at 19 sites evenly distributed along the horizontal centerline of the cavity. The end sensors are located one grid point away from the boundary wall, as seen in Fig. 2.

The controller is designed for disturbance rejection by the use of the model shown in Fig. 3. This model contains the open-loop dynamics as described by $\{V_m, \Phi, \Psi, P\}$. The weighting functions used for loop shaping are given as $\{W_p, W_n, W_k, W_y, W_h, W_u, W_d\}$. The mathematical objective of the control design is to choose a K such that the closed-loop transfer function from disturbances to errors has an induced norm less than unity for all plants within the parameter space.

The system has three input vectors and three output vectors. The inputs are the random noise $n \in \mathcal{R}^{19}$ that affect the sensor measurements, the exogenous disturbance $h \in \mathcal{R}$ that affects the upper boundary of the cavity, and the control input $u \in \mathcal{R}$ that affects the lower boundary of the cavity. The outputs are the frequency-domain weighted horizontal velocity measurements $e_1 \in \mathcal{R}^{19}$, the frequency-domain weighted control effort $e_2 \in \mathcal{R}$, and the sensor measurements $y \in \mathcal{R}^{19}$ used for feedback to the controller.

The open-loop dynamics consist of the cavity's velocity at the top, a control basis and flow shape basis. The part of the open-loop dynamics known as V_m is the mean velocity along the top of the cavity and has the equation $V_m = h_0(t)V_0$, where h_0 is the initial top disturbance and V_0 is a static Stokes flow along the top. The control basis for the plant takes the form $\Psi\beta(t)$, which was depicted as $\mathbf{g}(x, y)\beta(t)$ in the equations presented in the preceding sections, and coincides with the controlled velocity along the bottom of the cavity. The shape of the fluid flow within the cavity is determined by the flow shape basis Φ . The flow shape can take several forms; for example, the flow could be one large vortex circling the entire

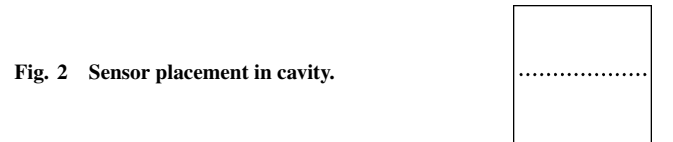


Fig. 2 Sensor placement in cavity.

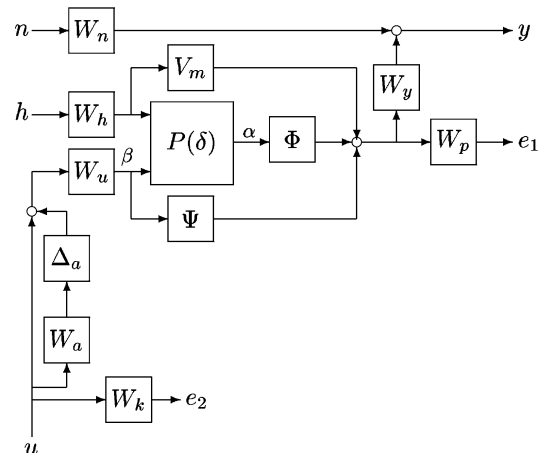


Fig. 3 Controller block diagram.

cavity, or two vortices of equal size with opposite rotation that meet along the horizontal centerline of the cavity.

The filter given as W_p serves to normalize the measurement of flow velocity collected by the sensors. This filter achieves loop-shaping that defines the design specifications in the frequency domain. The filter W_p is chosen to reflect the inverse of acceptable velocities in response to unity disturbances. The actual filter is realized as $W_p = 100$, which implies that the flow velocities should be less than 0.01 in the closed-loop system.

The filter W_k is used to normalize the penalty placed on the amount of actuation commanded by the controller. This filter reflects the capabilities of the actuation system. The magnitude of motion for the control actuator is allowed to be 0.2 in the nondimensional system. The weighting is chosen as the inverse so that $W_k = 5$.

The creation of a LPV controller requires that an output filter be used because a certain part of the observation matrix and feedthrough matrix vary with the different plants within the parameter space. The filter W_y is used as the output filter for this synthesis. The filter was chosen as $W_y = 1E5/(s + 1E5)$.

Also, the input matrix varies among the different plant models within the parameter space. This variation necessitates input filters within the synthesis. The filters shown as W_u and W_h are used as input filters and have the value of $1E5/(s + 1E5)$.

Multiplicative uncertainty was introduced into the control actuation to represent the effects of unmodeled dynamics and disturbances. The uncertainty is represented in the synthesis as Δ_a such that $\|\Delta_a\|_\infty \leq 1$. A weighting, $W_a = 0.2$, was used to limit the amount of uncertainty to 20% allowed into the control actuation.

Also, the filter W_n is included to account for noise that corrupts measurements by the sensors. The inclusion of noise is needed to provide a minimal level penalty on the sensors. The noise filter was chosen as $W_n = 0.001$, so that only a small amount of noise is considered by the control synthesis.

B. Synthesis

Robust controllers and an LPV controller have been designed for the system in Fig. 3. The techniques of \mathcal{H}_∞ control are used to reduce the induced norm from exogenous inputs to weighted errors.¹³ In this case, a set of individual controllers¹⁴ are designed for each model, along with a gain-scheduled LPV controller¹⁵ for all models.

Separate controllers are synthesized for each of the open-loop models based on excitation phase differentials. For each model, the same weightings are used to reflect the desirability of achieving the same performance level for each phase differential. The resulting induced norms achieved by the controllers are shown in Table 1.

The closed-loop norms are all greater than unity. Intuitively, these magnitudes imply that the controller is not able to achieve the desired performance and robustness objectives. Realistically, it must be kept in mind that there are 20 inputs and 20 outputs, creating a large number of transfer functions. This suggests that the magnitude of the norms is not unreasonable. The resulting closed-loop properties are studied in more detail shortly. It is shown that the large norms are caused by excessive control actuation. Essentially, the controller is not able to achieve the desired disturbance attenuation without exceeding the actuation limits. Fortunately, this violation is at low frequencies and is not expected to have a dramatic impact on the closed-loop simulations.

Also, the values in Table 1 are interesting in the sense that the induced norms increase as the level of phase differential increases. Such behavior indicates that the excitation phase differential does

indeed have a large impact on the fluid dynamics. The increasingly poor performance of the controllers demonstrates that the flow modes for a phase differential of 210 deg have properties that are more difficult to control than those for a phase differential of 150 deg, for example.

The last entry in Table 1 is the norm associated with the LPV controller. When the phase differential is allowed to be time-varying, the norm increases as expected. Note that this norm did not raise much above the norm associated with the \mathcal{H}_∞ controller for the 210-deg phase differential model. This condition indicates that the LPV controller is able account for the time-varying nature of the phase differential without excessive loss of performance.

VI. Simulation

A. Open-Loop Simulation

A series of open-loop simulations are performed to demonstrate the fluid qualitative response resulting from the disturbance for both full-order and reduced-order models. These simulations are similar in the sense that the same magnitude of disturbance is used for the boundary conditions on the top of the domain. Conversely, the simulations involving the reduced-order models differ in that the flow on the bottom boundary has different values of phase lag with respect to the flow on the top boundary.

The flow conditions resulting from these simulations are visualized to demonstrate the dynamics. The data in Figs. 4–16 present the horizontal velocity as a function of time. In each case, the data are three-dimensional to show the velocity measured at each of the 19 sensors as a function of time.

Again, note that all measurements are nondimensional. This characteristic applies to both the time and velocity component, and so no units are noted for the simulations.

The open-loop flow for the full-order model is used as a comparison for the reduced-order model simulations and is shown in Fig. 4. Figure 4 clearly shows the sinusoidal nature of the flow that results from the top exogenous disturbance changing with a sine function, $h_0(t) = \sin(2\pi t)$. The flow near the center of the cavity, near point 11, shows the largest velocity with a magnitude near -0.2 at $t = 0.3$ to $+0.2$ at $t = 0.7$.

The flow for the reduced-order model with a phase differential of 165 deg is shown in Fig. 5. Figure 5 also demonstrates a sinusoidal nature, but has a smaller open-loop magnitude compared to the full-order flow with the highest velocity being 0.07.

The flow for the reduced-order model with an phase differential of 210 deg is shown in Fig. 6. The flow again demonstrates a sinusoidal nature, and the velocities are slightly larger than those of the full-order model.

A sinusoidal trajectory of phase differentials shown in Fig. 7 is used in a simulation that shows the open-loop characteristics of the reduced-order flow as phase differential changes.

The flow velocities for the reduced-order model throughout the time-varying phase trajectory are shown in Fig. 8. The sinusoidal nature that is apparent in all of the other open-loop flows is slightly different for this open-loop flow. This difference is due to the changing of the parameter through the trajectory. The formation of the full-order flow involved the bottom of the cavity being allowed to

Table 1 Induced norms of closed-loop system

Phase differential, deg	\mathcal{H}_∞ norm
150	7.475
165	8.177
180	7.647
195	10.143
210	10.829
150–210	12.785

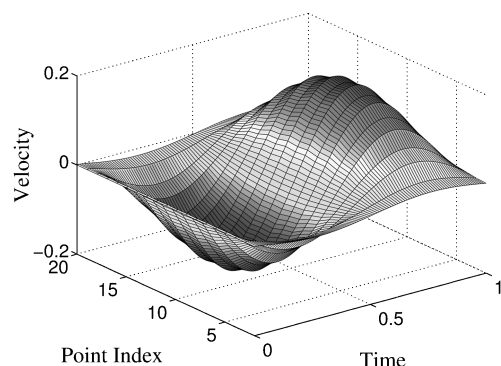


Fig. 4 Open-loop flow velocities for full-order model.

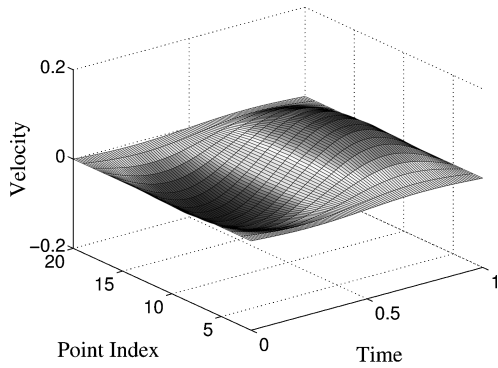


Fig. 5 Open-loop flow velocities for reduced-order model with 165-deg phase differential.

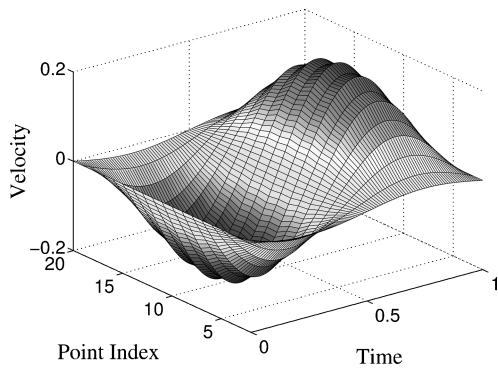


Fig. 6 Open-loop flow velocities for reduced-order model with 210-deg phase differential.

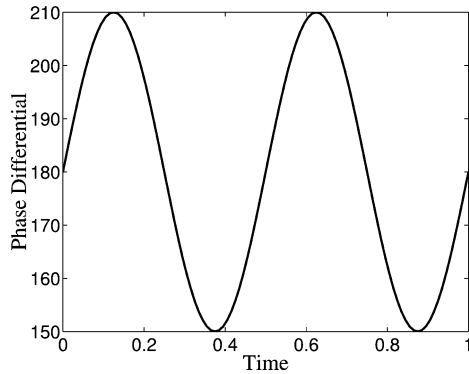


Fig. 7 Trajectory of phase differential.

move freely. As a result, the full-order flow incorporates all phase differentials. This feature makes the full-order flow have no dependence on phase differential; therefore, the velocities for the full-order model's flow over the phase differential trajectory are the same as those plotted in Fig. 4.

Note that the flow for each reduced-order model with phase differential has a similar shape, but significantly different magnitude. The maximum velocity measured at the center of the cavity is smaller in magnitude for the models with phase differentials located at the beginning of the range than the models with phase differentials near the end of the range. This feature indicates the flow is indeed strongly dependent on phase differential; therefore, phase differential should be considered for control design.

B. Reduced-Order Closed-Loop Simulation

The closed-loop dynamics are also simulated to demonstrate the performance of the controller for the reduced-order models in this section and for the full-order model in the next section. The diagram of the closed-loop system for both the reduced-order models and the full-order model is shown in Fig. 9. These simulations use the same open-loop dynamics, but include the LPV controller that was

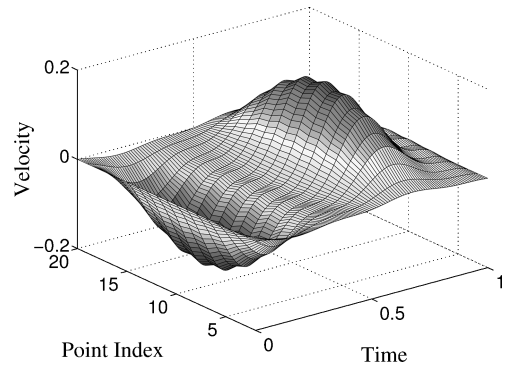


Fig. 8 Open-loop flow velocities for reduced-order model over a trajectory of phase differentials.

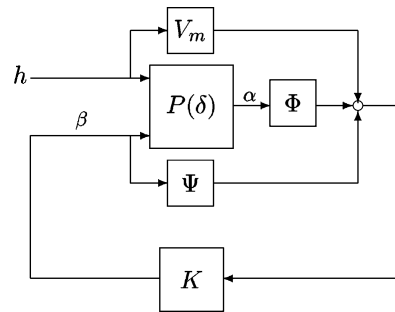


Fig. 9 Closed-loop system.

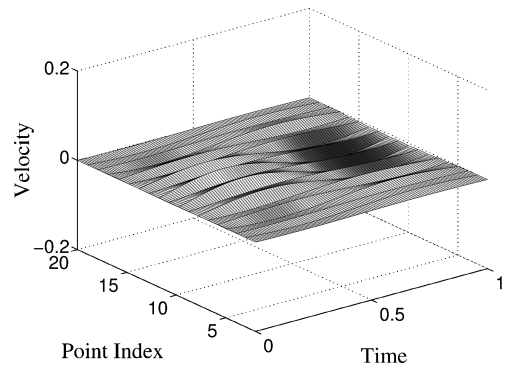


Fig. 10 Closed-loop flow velocities for reduced-order model with 165-deg phase differential.

synthesized over the range of phase differentials, which contains 24 states. In each simulation, the flow on the upper boundary is the same, but now the flow on the lower boundary results only from the commands issued by the controller. In this section, the controller was tested with reduced-order models for two specific cases of phase differential and over a time-varying trajectory of phase differentials.

The measured velocities for the reduced-order model with a phase differential of 165 deg in response to the LPV controller with a phase differential of 165 deg is shown in Fig. 10. The comparison of these velocities with the open-loop measurements in Fig. 5 demonstrate a reduction of velocity along the center of the cavity, where the velocity is greatest, of roughly 70%.

The measured velocities for the reduced-order model with a phase differential of 210 deg in response to the LPV controller with a phase differential of 210 deg is shown in Fig. 11. The reduction in velocities is apparent by comparison of the closed-loop velocities in Fig. 11 with the open-loop velocities in Fig. 6, which shows a reduction along the center of the cavity of roughly 90%.

The closed-loop simulation of the reduced-order models over the phase differential trajectory, which also affects the LPV controller, is shown in Fig. 12. The velocity magnitude shows a clear reduction in magnitude compared to the open-loop simulation of flow over

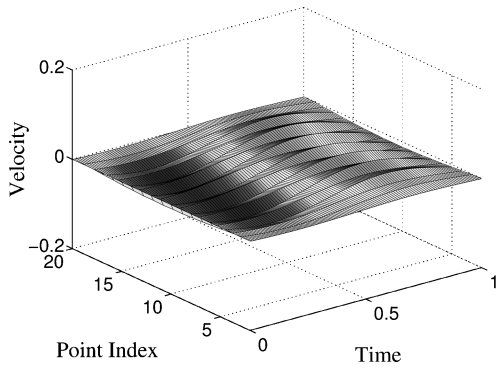


Fig. 11 Closed-loop flow velocities for reduced-order model with 210-deg phase differential.

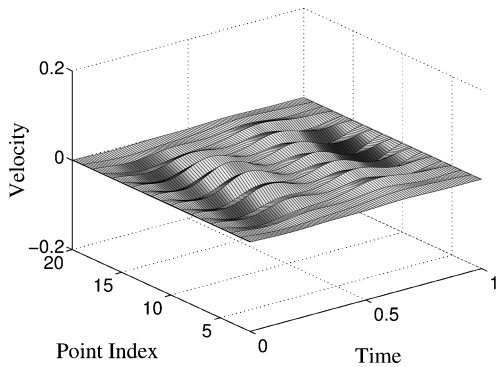


Fig. 12 Closed-loop flow velocities for reduced-order model over a trajectory of phase differentials.

the phase differential trajectory, which was shown in Fig. 8. The reduction along the center is roughly 80%.

The disturbance rejection is significant for the LPV controller with the reduced-order models. These reductions confirm that the LPV controller will work not only for reduced-order models at specific phase differentials, but also over a time-varying trajectory of phase differentials. The simulations did show some differences between each of the reduced-order models. In particular, the amount of attenuation was slightly less for the reduced-order model with a phase differential of 165 deg, but much higher for the reduced-order model with a phase differential of 210 deg. This decrease in attenuation seems almost contradictory, given that the open-loop simulations showed a decrease in flow velocities for the same models. The cause of this phenomenon may be the controller not being able to reduce the lower-phase differential models' velocity magnitude by a large percentage due to their smaller open-loop velocity magnitude.

C. Full-Order Closed-Loop Simulation

The simulations that were performed for the reduced-order models were repeated with the full-order model. The reduced-order models are subscales of this full-order model, and so the performance of the controllers on the full-order model is actually of predominant interest.

The measured velocities in response to an \mathcal{H}_∞ controller, created specifically for the full-order model, are shown in Fig. 13. Clearly, the magnitude of the velocity is dramatically decreased below the open-loop level. The velocities in Fig. 13 are several orders of magnitude less than the corresponding open-loop velocities in Fig. 4. This response will be used as a comparison for the responses from the full-order model controlled by the LPV controller.

The velocities for the full-order model in response to the LPV controller with a phase differential of 165 deg is shown in Fig. 14. Though the velocities were not reduced to the extent of the full-order simulation in Fig. 13, they were reduced by an amount comparable to the response shown by the reduced-order model at a 165-deg phase

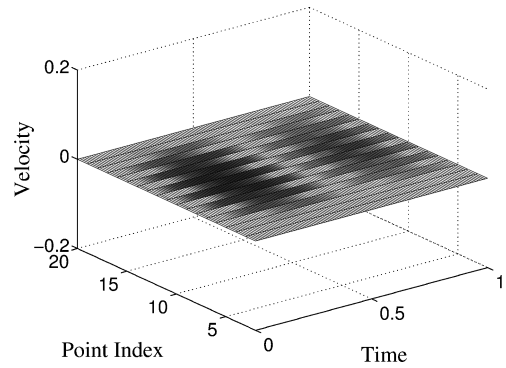


Fig. 13 Closed-loop flow velocities for full-order model.

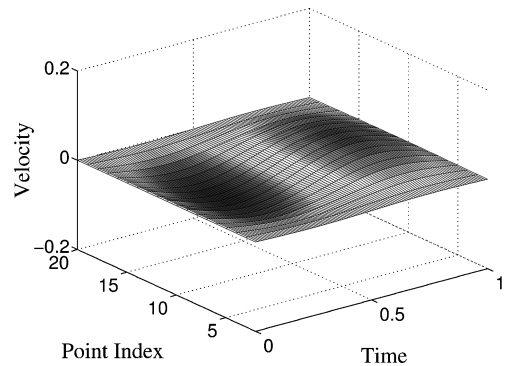


Fig. 14 Closed-loop flow velocities for full-order model with controller associated with 165-deg phase differential.

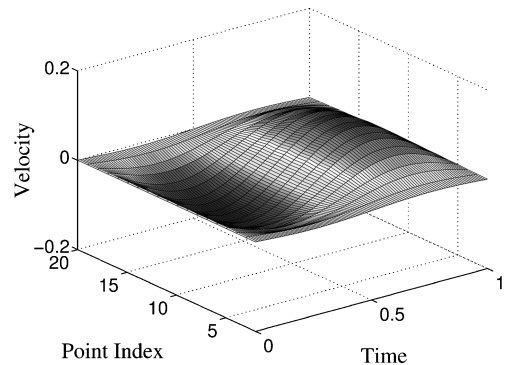


Fig. 15 Closed-loop flow velocities for full-order model with controller associated with 210-deg phase differential.

differential. The reduction in the velocity magnitude is evident along the center of the cavity and is roughly 80%.

The velocity magnitudes for the full-order model in response to the LPV controller for a phase differential of 210 deg is shown in Fig. 15. The reduction in velocity compared to the open-loop flow of the full-order flow in Fig. 4 is very clear. The velocities along the centerline of the cavity were reduced by 60%. Though the velocities were not reduced as much as those in the simulation in Fig. 13, the velocities were reduced by an amount comparable to the reduced-order model at a 210-deg phase differential.

The closed-loop simulation of the full-order model controlled by the LPV controller over the phase differential trajectory is shown in Fig. 16. The velocities show a clear reduction in magnitude compared to the open-loop full-order flow in Fig. 4. The flow along the center of the cavity is reduced by 66%.

The disturbance rejection is significant for both the reduced-order models and the full-order model. These reductions confirm that the LPV controller, created for a phase differential parameter, will work not only for the reduced-order models, which are dependent on phase differential, but also for the full-order model.

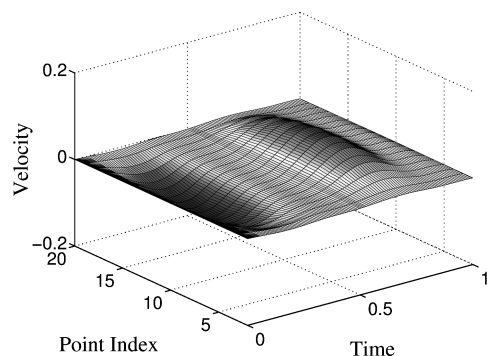


Fig. 16 Closed-loop flow velocities for full-order model over a trajectory of phase differentials.

VII. Conclusions

Flow control is an exceedingly difficult challenge because of the nonlinearities and time variations inherent in flowfields. These inherent difficulties can be avoided when the flow to creeping Stokes flow within a driven cavity, is restricted. This paper has introduced a control methodology suitable for such a system. In particular, the controllers are designed under consideration of subspaces of the flowfield that describe modes associated with phase differential between exogenous disturbances. The models of these subspaces are realized as state-space systems, and a controller can be designed that uses the LPV framework. The resulting controller is shown to decrease the flow velocities within the cavity significantly for both the reduced-order subspaces, which have single phase differentials, and also for the full-order flow, which encompasses all phase differentials.

References

¹Chih-Ming, H., "Control of Fluid Flows by Micro Transducers," *International Symposium on Micro Machine and Human Science*, IEEE Publica-

tions, Piscataway, NJ, 1996, pp. 29–33.

²Ortiz, J., and Barhorst, A., "Modeling Fluid–Structure Interaction," *Journal of Guidance, Control, and Dynamics*, Vol. 20, No. 6, 1997, pp. 1221–1228.

³Ito, K., and Ravindran, S. S., "A Reduced Order Method for Control of Fluid Flows," *Conference on Decision and Control*, Vol. 4, IEEE Publications, Piscataway, NJ, 1996, pp. 3705–3710.

⁴Burns, J. A., and Yuh-Roung, O., "Feedback Control of the Driven Cavity Problem Using LQR Designs," *Conference on Decision and Control*, Vol. 1, IEEE Publications, Piscataway, NJ, 1994, pp. 289–294.

⁵Banks, H. T., and Ito, K., "Structural Actuator Control of Fluid/Structure Interactions," *Conference on Decision and Control*, Vol. 1, IEEE Publications, Piscataway, NJ, 1994, pp. 283–288.

⁶Rediniotis, O. K., Ko, J., Yue, X., and Kurdila, A. J., "Synthetic Jets, Their Reduced Order Modeling and Applications to Flow Control," AIAA Paper 99-1000, Jan. 1999.

⁷Ravindran, S. S., "Reduced-Order Adaptive Controllers for MHD Flows Using Proper Orthogonal Decomposition," *Conference on Decision and Control*, Vol. 3, IEEE Publications, Piscataway, NJ, 2001, pp. 2454–2459.

⁸Feng, Y., Kurdila, A. J., Lind, R., and Mikolaitis, D. W., "Linear Parameter-Varying Flow Control for a Driven Cavity Using Reduced-Order Models," AIAA Paper 2003-5351, Aug. 2003.

⁹Lumley, J., "The Structure of Inhomogeneous Turbulent Flows," *Atmospheric Turbulence and Radio Wave Propagation*, edited by A. M. Yaglom and V. I. Tararsky, Nauka, Moscow, 1967, pp. 166–178.

¹⁰Baramov, L., Tutty, O., and Rogers, E., "Robust Control of Linearized Poiseuille Flow," *Journal of Guidance, Control, and Dynamics*, Vol. 25, No. 1, 2002, pp. 145–151.

¹¹Ji, L., and Zhou, J., "The Boundary Element Method For Boundary Control of The Linear Stokes Flow," *Conference on Decision and Control*, Vol. 3, IEEE Publications, Piscataway, NJ, 1990, pp. 1192–1194.

¹²Coimbra, C. F. M., and Rangel, R. H., "Spherical Particle Motion in Unsteady Viscous Flows," AIAA Paper 99-1031, Jan. 1999.

¹³Zhou, K., Doyle, J. C., and Glover, K., *Robust and Optimal Control*, Prentice–Hall, Upper Saddle River, NJ, 1996, pp. 449–476.

¹⁴Balas, G. J., Doyle, J. C., Glover, K., Packard, A., and Smith, R., *μ -Analysis and Synthesis Toolbox*, MathWorks, Natick, MA, 2001, pp. 3.16–3.19.

¹⁵Gahinet, P., Nemirovski, A., Laub, A. J., and Chilali, M., *LMI Control Toolbox*, MathWorks, Natick, MA, 1995, pp. 7.1–7.10.